Journal of Atmospheric and Solar-Terrestrial Physics 149 (2016) 180–190

Contents lists available at ScienceDirect

Journal of Atmospheric and Solar-Terrestrial Physics

journal homepage: www.elsevier.com/locate/jastp

The influence of Middle Range Energy Electrons on atmospheric chemistry and regional climate

P. Arsenovic [a,*], E. Rozanov [a,b], A. Stenke [a], B. Funke [c], J.M. Wissing [d], K. Mursula [e], F. Tummon [a], T. Peter [a]

[a] Institute for Atmospheric and Climate Science ETH, Zürich, Switzerland
[b] Physikalisch-Meteorologisches Observatorium Davos – World Radiation Center, Davos, Switzerland
[c] Instituto de Astrofisica de Andalucia, CSIC, Granada, Spain
[d] Universität Osnabrück, Lower Saxony, Germany
[e] ReSoLVE Centre of Excellence, Oulu, Finland

ARTICLE INFO

Article history:
Received 27 December 2015
Received in revised form
11 April 2016
Accepted 12 April 2016
Available online 13 April 2016

Keywords:
Middle Energy Electrons
Mesosphere
Ozone
Atmospheric Chemistry
Climate

ABSTRACT

We investigate the influence of Middle Range Energy Electrons (MEE; typically 30-300 keV) precipitation on the atmosphere using the SOCOL3-MPIOM chemistry-climate model with coupled ocean. Model simulations cover the 2002-2010 period for which ionization rates from the AIMOS dataset and atmospheric composition observations from MIPAS are available. Results show that during geomagnetically active periods MEE significantly increase the amount of NO_y and HO_x in the polar winter mesosphere, in addition to other particles and sources, resulting in local ozone decreases of up to 35%. These changes are followed by an intensification of the polar night jet, as well as mesospheric warming and stratospheric cooling. The contribution of MEE also substantially enhances the difference in the ozone anomalies between geomagnetically active and quiet periods. Comparison with MIPAS NO_y observations indicates that the additional source of NO_y from MEE improves the model results, however substantial underestimation above 50 km remains and requires better treatment of the NO_y source from the thermosphere. A surface air temperature response is detected in several regions, with the most pronounced warming occurring in the Antarctic during austral winter. Surface warming of up to 2 K is also seen over continental Asia during boreal winter.

1. Introduction

Energetic particles are one of the natural factors closely related to solar activity that can directly impact the chemical composition of the upper atmosphere. They can directly impact temperature and dynamics and can also have an indirect effect on polar surface temperatures (Seppälä et al., 2009; Rozanov et al., 2012). Their contribution to climate change is, however, not well established and typically not included in climate change assessments such as the 2013 Intergovernmental Panel on Climate Change (IPCC report, 2013).

Depending on their source and energy, energetic particles can be divided into five categories: galactic cosmic rays (GCR), solar energetic protons (SEP), low energy (auroral or plasmasheet) electrons (LEE), and middle and high energy (Van Allen radiation belt) electrons (MEE and HEE). GCR originate from outside of our solar system and consist largely of protons, ~10% helium nuclei and ~1% other elements, with energies ranging from about 1 MeV up to 5×10^{13} MeV (Grieder, 2001; Dorman 2004). Ionization by GCR maximizes at around 15 km altitude (Usoskin et al., 2010) over the polar areas and gradually decreases towards the equator. SEP originate from solar flares, coronal mass ejections, and accompanied interplanetary shocks. They occur as sporadic events and their kinetic energy is typically up to 500 MeV (Reames 1999; Cane et al. 2006). Ionization by SEPs is most pronounced in the Polar Regions (Jackman et al., 2008) and maximizes in the upper stratosphere. Energetic electrons originate from the solar wind and they can be trapped in the terrestrial magnetosphere (LEE), forming the aurora, or trapped in the outer Van Allen radiation belt where they can get accelerated during geomagnetic substorms and precipitate into the atmosphere (MEE and HEE) (Sinnhuber et al., 2012). LEE (< 30 keV) precipitate into the atmosphere from the Earth's magnetospheric plasmasheet (Brasseur and Solomon, 2005) and ionize neutral molecules above 90 km

* Correspondence to: Institute for Atmospheric and Climate Science ETH, Universitätstrasse 16, 8092 Zürich, Switzerland.
E-mail address: pavle.arsenovic@env.ethz.ch (P. Arsenovic).

http://dx.doi.org/10.1016/j.jastp.2016.04.008

altitude inside the auroral oval (roughly 55°–70° geomagnetic latitude), but they are not capable of penetrating to lower latitudes (Baker et al. 2001; Barth et al. 2003). MEE precipitate continuously from the radiation belt (energies varying from 30 to 300 keV) by spiraling down into the sub-auroral zone and ionize neutral molecules (N_2 and O_2) mostly between 70 and 90 km altitude to produce nitrogen and hydrogen oxide radicals (Rusch et al., 1981; Solomon et al., 1981; Aikin 1994; Turunen et al., 2009; Egorova et al., 2011), which are known to deplete ozone in catalytic destruction cycles (Brasseur and Solomon, 2005). Finally, HEE (300 keV – several MeV) precipitate from the outer radiation belt and affect atmospheric chemistry below 70 km altitude (e.g., Bazilevskaya et al. 2008; Turunen et al., 2009).

Study of the lower thermosphere, mesosphere, and stratosphere essentially started in the second half of the 20th century. The chemical composition of the middle atmosphere and thermosphere was investigated using in situ measurements and remote sensing instruments and it has since become apparent that energetic particle precipitation can significantly influence atmospheric chemistry above the tropopause (e.g., Nicolet 1965, 1975; Weeks et al., 1972; Swider and Keneshea, 1973; Crutzen 1975; Solomon et al., 1982). The influence of energetic particles on the ozone layer and climate is a relatively new area of research. The effects of GCR have been analyzed by (Calisto et al., 2011), Semeniuk et al., (2011), and more recently by Jackman et al. (2015). The simulated and observed effects of energetic SEP on the atmosphere have been widely presented in the literature (e.g., Jackman et al., 2009; Funke et al., 2011). Several groups have studied the influence of LEE. Baumgaertner et al. (2009) and Rozanov et al. (2012) applied state-of-the-art chemistry-climate models (CCM) and demonstrated that LEE substantially affect the ozone layer, stratospheric dynamics, as well as tropospheric climate during the cold season. However, these models did not include MEE and HEE electrons, which can underestimate the importance of energetic particles.

One of the first attempts to estimate the influence of MEE on the atmosphere was undertaken by Codrescu and Fuller-Rowell (1997). They used data obtained from the TIROS/NOAA polar orbiting satellites to characterize precipitating protons and electrons with energies in the range of 30 keV–2.5 MeV and used these data as inputs for the National Center for Atmospheric Research (NCAR) thermosphere ionosphere mesosphere electrodynamic general circulation model (TIME-GCM). They showed that MEE and HEE together significantly increased NO_x ($[N]+[NO]+[NO_2]$) and HO_x ($[H]+[OH]+[HO_2]$) leading to ozone loss of up to 27% between 70 and 80 km. This was in turn followed by small changes in temperature and wind. However, the potential climate effects of MEE were not considered in this work. Among others, a modeling study on energetic electrons was carried out using the Canadian Middle Atmosphere Model (CMAM; Semeniuk et al. 2011). They used electron flux data from the Medium Energy Proton and Electron Detector (MEPED) for the period 1979-2006. The energy range of the electron data used in their model was 30–1000 keV and ionization rates were calculated using a simplified energy deposition code. Their results revealed significant increases of NO_x and HO_x in the mesosphere and upper stratosphere, which led to average mesospheric ozone depletion of up to 60% (80%) for boreal (austral) winter for the simulated period. These changes in ozone in turn influenced atmospheric temperature and dynamics. However, their experiments did not include the NO_x produced by LEE resulting in low NO_x mixing ratios in the upper stratosphere/mesosphere and an underestimation of the relative ozone depletion.

Limited understanding of MEE and their properties is reflected in the absence of reliable model parameterizations for the ionization induced by these particles. MEE precipitation into atmosphere is associated with high speed solar wind streams (Baker et al., 1993), which are most frequent during the declining phase of the solar cycle. On the other hand, a possible future grand solar minimum (Steinhilber and Beer, 2013) would lead to suppression of geomagnetic activity and a decrease in electron precipitation. In this case, the absence of MEE in models could result in an overestimation of the ozone increase in future, with consequent implications for climate. The direct ionizing effect leading to NO_x and HO_x production is constrained to the mesosphere. HO_x is short-lived (lifetime of seconds-hours), while NO_x has a longer lifetime (days-months). Therefore, HO_x is more important near its production region in the mesosphere while NO_x can be transported in the polar vortex (Solomon et al., 1982) to the stratosphere, inducing ozone depletion through catalytic chemical cycles. Ozone decreases lead to reduced heating and thus alters atmospheric dynamics, i.e. perturbations which may impact all the way down to the troposphere and Earth's surface (Baumgaertner et al., 2011).

Recent progress in the calculation of ionization rates (Wissing and Kallenrode, 2009) makes it possible to consider MEE in global climate models. Furthermore, the availability of accurate observations of atmospheric composition (e.g., Funke et al., 2014; Andersson et al., 2014 can be used to validate model results.

2. Methods

We use the coupled chemistry-climate model SOCOL3-MPIOM (Stenke et al., 2013; Muthers et al., 2014), which consists of the general circulation model ECHAM5.4 (Roeckner et al., 2003) coupled to the chemistry module MEZON (Rozanov et al., 1999; Egorova et al., 2003) and the MPIOM ocean model (Marsland, 2003; Jungclaus et al., 2006). Parameterizations of GCR, SEP, and LEE were introduced identically as in Rozanov et al. (2012) and Anet et al. (2013). GCR ionization rates are parameterized as a function of geomagnetic latitude, pressure, and solar modulation potential. Daily vertical profiles of solar proton ionization rates are taken from Jackman et al. (2008), while the NO_x flux into the model domain from the auroral zone is parameterized using the geomagnetic disturbance A_p index (Baumgaertner et al., 2009). HEE are not implemented due to the lack of an available parameterization.

The treatment of MEE in this model version is based on ionization rates obtained from the AIMOS version 1.6 dataset. AIMOS (Wissing and Kallenrode, 2009) is a 3D numerical model designed to calculate atmospheric ionization rates from energetic particle precipitation. AIMOS exploits a Monte Carlo approach and a sorting algorithm to assign observations from POES-15/16 and GOES-10/11 satellites to horizontal precipitation cells, depending on geomagnetic activity. The AIMOS data includes electrons, SEP, and alpha particles for the period 2002–2010. The highest MEPED electron channel, measuring electrons with energies exceeding 300 keV, is not included in the dataset as it does not have a proper upper energy range and is also contaminated (Yando et al., 2011). During periods of high proton flux, MEPED electron channels are not used at all. The electron energy range is 30-300 keV and unlike in previous versions where a positive bias was observed, there is no apparent overestimation of the electron ionization rate in version 1.6. In order to investigate the influence of MEE, we use daily ionization rates below 0.01 hPa (~80 km) from precipitating electrons.

Fig. 1a shows the hemispheric average of monthly mean ionization rates at 0.01 hPa. The period considered is characterized by different levels of solar and geomagnetic activities: the time period from 2002 to 2005 was rather active and characterized by very intense ionization, while after 2005 geomagnetic activity decreased, leading to lower ionization rates. Ionization rates in the Southern Hemisphere are higher than in the Northern Hemisphere

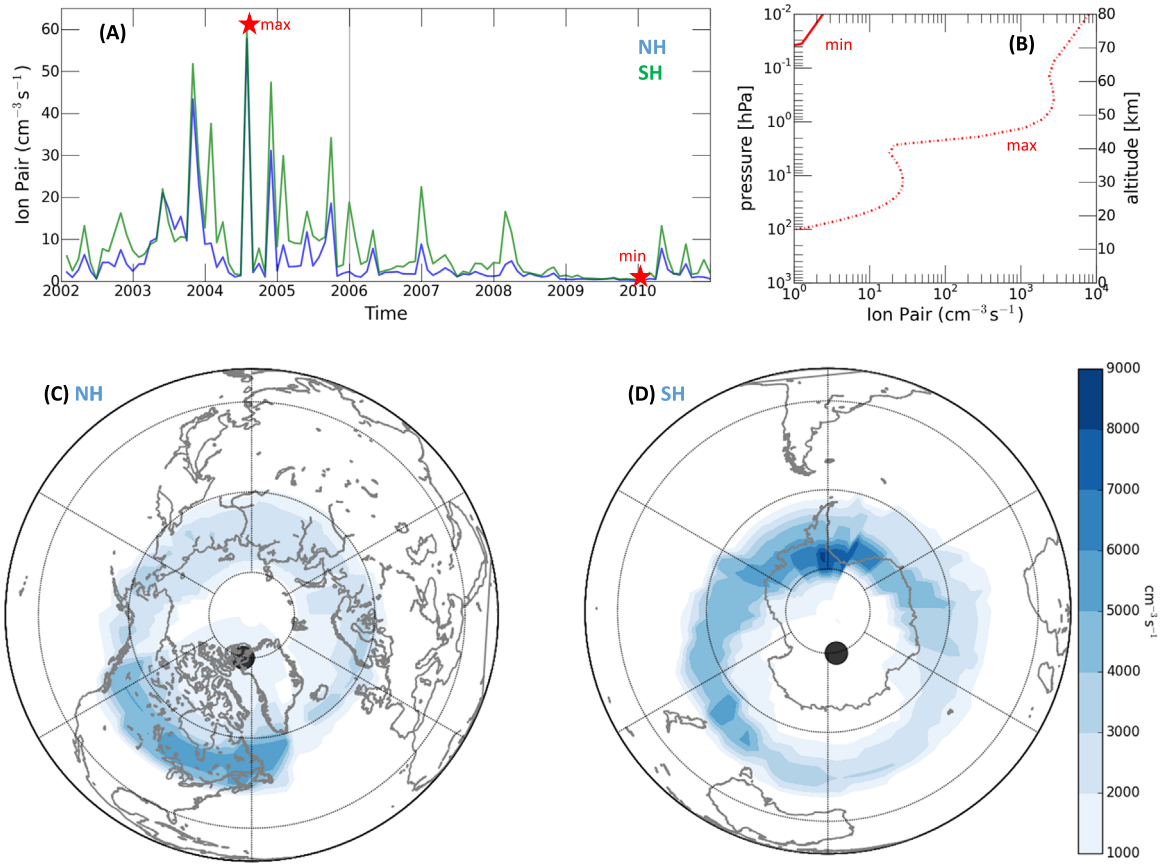

Fig. 1. (A) Monthly and global mean ionization rates at 0.01 hPa (~80 km altitude). The vertical line separates periods of high (2002–2005) and low (2006–2010) geomagnetic activity. The blue (green) line: Northern (Southern) Hemisphere mean values while red stars indicate maximum and minimum ionization rates, (July 2004 and January 2010, respectively). (B) – Vertical profiles of the peak daily ion pair production. The dash-dot (solid) line represents maximum (minimum) daily ionization rates for the 2002–2010 (October 28, 2003 and January 1, 2010, respectively). (C), (D) – Daily mean maximum ionization rates for the Northern (C) and Southern (D) Hemisphere for October 28, 2003. The black dot indicates the location of the geomagnetic pole (following Finlay et al., 2010). (For interpretation of the references to color in this figure legend, the reader is referred to the web version of this article.)

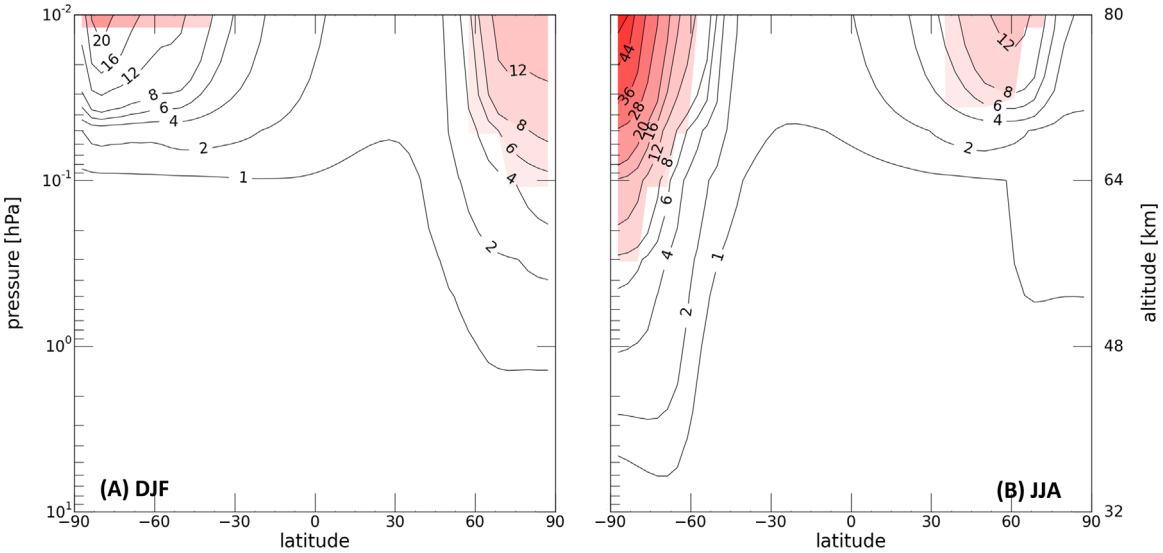

Fig. 2. Zonal mean NO_x difference (MEE — NOMEE) in ppbv for DJF (A) and JJA (B), averaged over the 2002–2005 period. Colored regions are significant at the 95% confidence level (calculated using a Student *t*-test). (For interpretation of the references to color in this figure legend, the reader is referred to the web version of this article.)

at any time of the covered period. The red stars in Fig. 1a show the maximum and minimum monthly mean values of ionization rates, while the maximum and minimum vertical profiles of daily peak are shown in Fig. 1b. The maximum values appear in the second half of 2004 while minimum values are observed at the beginning of 2010. Ionization rates are highest at the model top (0.01 hPa) and decrease with altitude. The maximum ionization rate is four orders of magnitude higher than the minimum values. It should be noted that the magnitude of the applied ionization rates are up to ten times smaller than in Semeniuk et al. (2011).

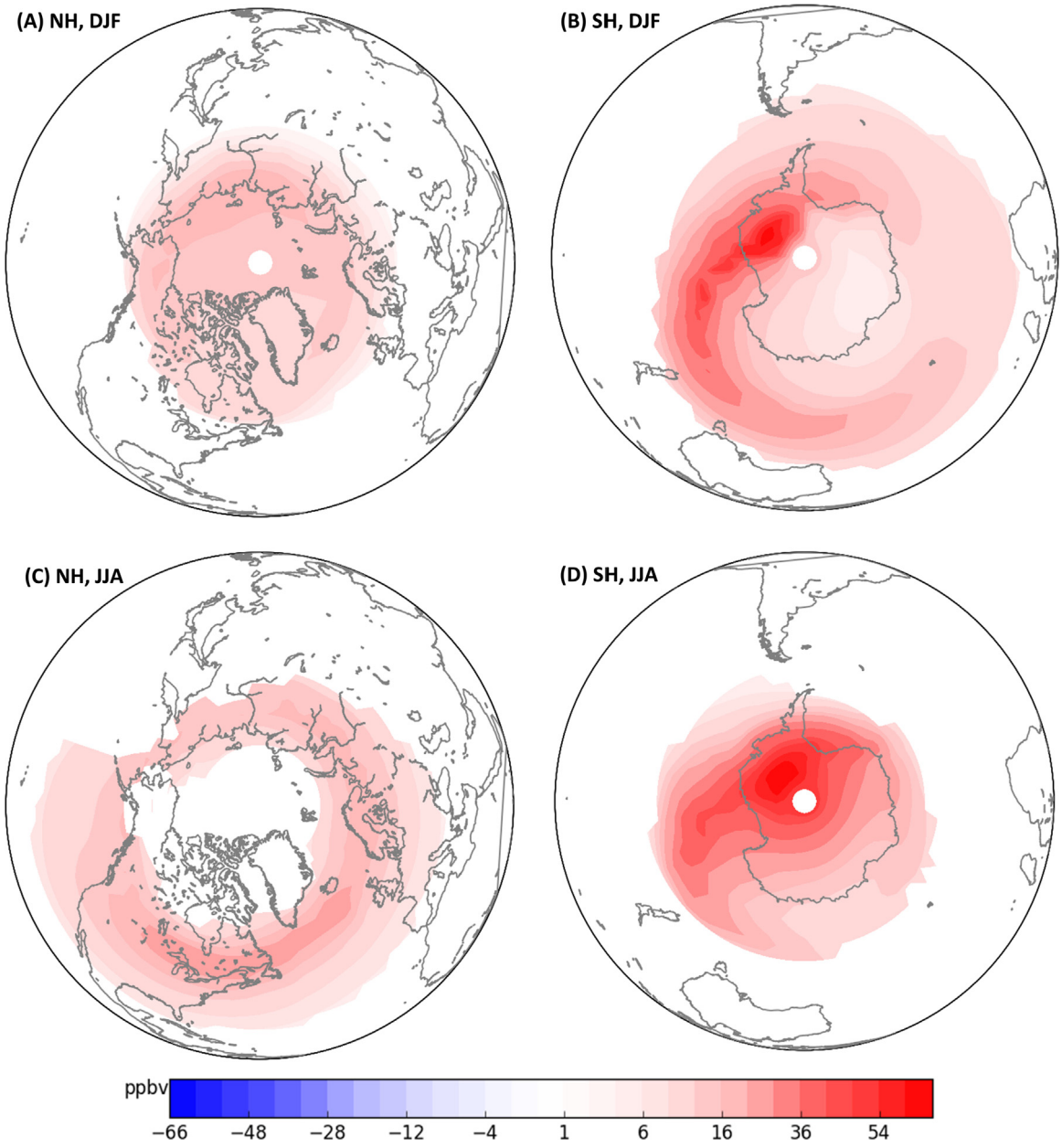

Fig. 3. Monthly mean response of NO_x (ppbv) to MEE at 0.01 hPa (averaged for 2002-2005). (A) Boreal winter (DJF). (B) Austral summer (DJF). (C) Boreal summer (JJA). (D) Austral winter (JJA). Colored regions are at 95% confidence level (calculated using a Student *t*-test). (For interpretation of the references to color in this figure legend, the reader is referred to the web version of this article.)

The geographic distribution of maximum ionization rates at 0.01 hPa is shown in Fig. 1c and d. The maximum electron ionization rates that occur on 28 October 2003 coincide with the one of the largest solar proton events of the past thirty years (Degestin et al., 2005). The center of the auroral oval is located at the geomagnetic pole (black dot in the Fig. 1c and d, following Finlay et al., 2010), and the asymmetric spatial distribution is caused by the drift of the loss cone. Electrons gyrate along the Earth's magnetic field lines, bouncing from pole to pole. As they do so, some electrons get lost when they enter denser air at the poles. This loss intensifies when the magnetic field weakens in the area of the South Atlantic Anomaly (SAA) and particle precipitation therefore intensifies at the foot-points of the field lines crossing the SAA. The southern position of the SAA also causes the observed hemispheric asymmetry.

In the model ionization rates are converted to NO_x and HO_x production rates by assuming that 1.25 nitrogen atoms are produced per ion pair, from which 45% is ground-state atomic nitrogen and 55% is $N(^2D)$, which instantaneously convert to NO. The number of HO_x particles produced per ion pair is parameterized as a function of altitude and ionization rate for daytime, polar summer conditions of temperature, air density, and solar zenith angle. This simplified treatment of NO_x and HO_x production in the mesosphere and upper stratosphere has been widely applied for the study of energetic particle effects on the atmosphere (e.g., Jackman et al., 2008; Funke et al., 2011; Semeniuk et al., 2011; Rozanov et al., 2012). This approach has been evaluated by comparison with more detailed treatments of the ion chemistry by Egorova et al. (2011) and Nieder et al., (2014). These studies confirmed that the accuracy of this approach is within 10–20% up to about 80 km altitude, for most of the species considered, including ozone. However, the production of HNO_3 driven by ion recombination cannot be properly reproduced.

We performed two ensemble experiments covering the 2002–

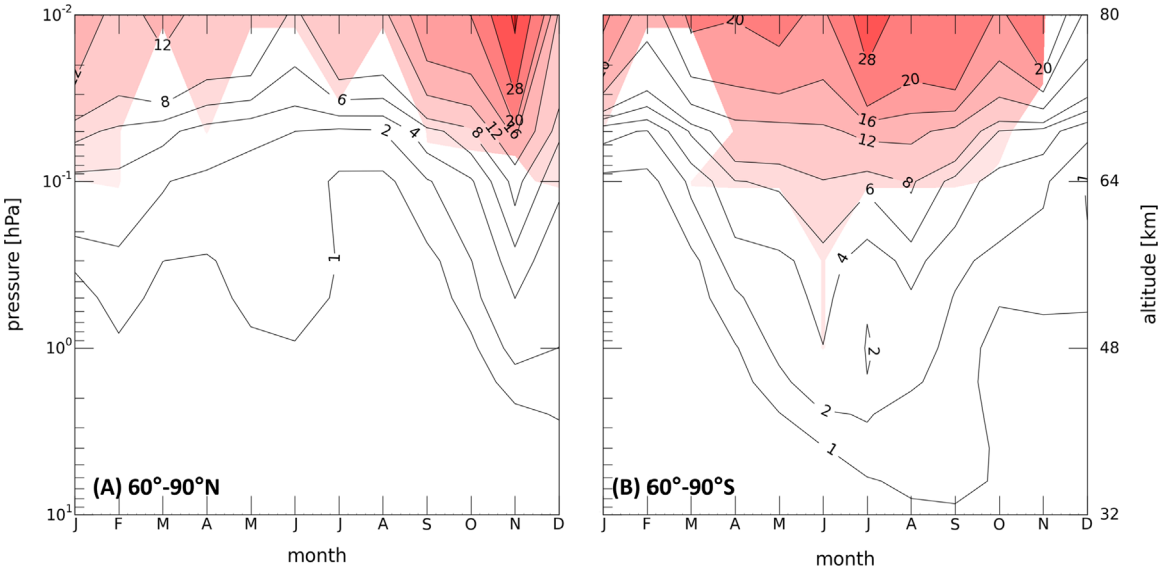

Fig. 4. Monthly zonal mean response of NO_x, (ppbv) to MEE averaged over 60°–90 °N (A) and 60°–90 °S (B), calculated for 2002–2005. Colored areas are significant at the 95% confidence level (calculated using a Student *t*-test). (For interpretation of the references to color in this figure legend, the reader is referred to the web version of this article.)

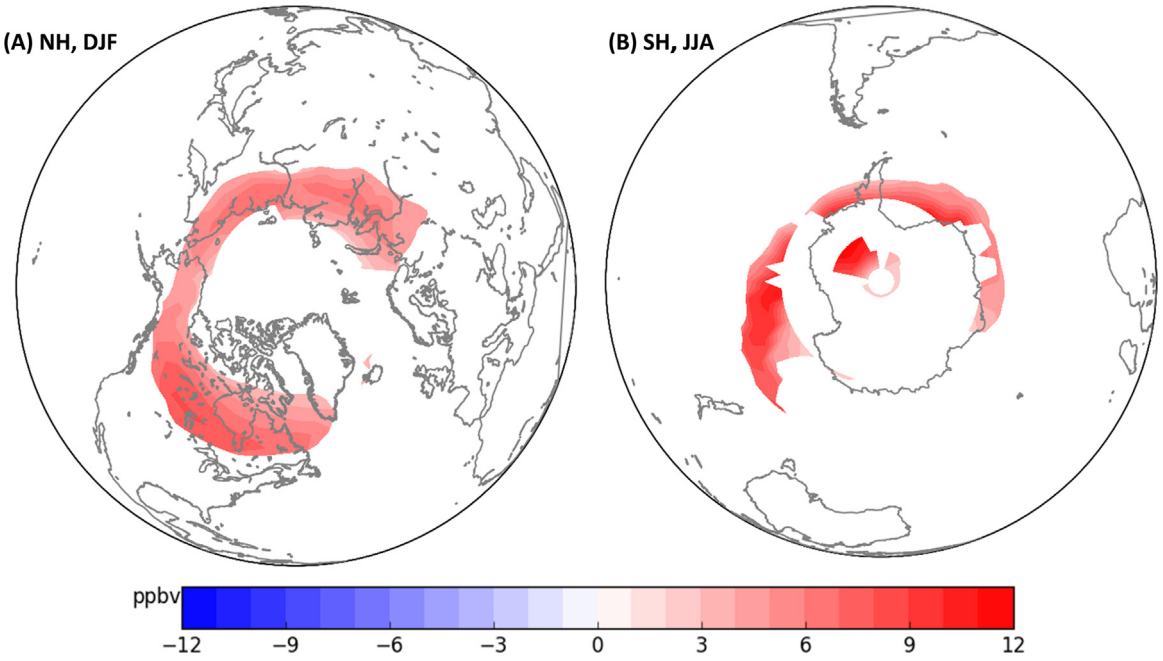

Fig. 5. Monthly mean response of HO_x (ppbv) to MEE at 0.01 hPa (averaged over 2002–2005). Boreal (DJF) and (B) Austral (JJA) winter. Colored regions are significant at the 95% confidence level (calculated using a Student *t*-test). (For interpretation of the references to color in this figure legend, the reader is referred to the web version of this article.)

2010 period using our standard model configuration with approximately 3.75° horizontal resolution and 39 vertical levels from the surface up to 0.01 hPa (Muthers et al., 2014). The reference ensemble (hereafter referred to as NOMEE) consists, in terms of particles, of GCR, SEP, and LEE. The experiment (termed MEE) in addition includes MEE ionization rates from AIMOS. All other forcing data (solar irradiance, aerosols, greenhouse gases, ozone depleting substances, quasi-biennial oscillation) are kept the same between the experiments. Solar irradiance follows the 11-year solar cycle. Tropospheric aerosols are adapted from CAM3.5 simulations, while stratospheric aerosols are kept at background levels. Concentrations of greenhouse gases (GHGs) and ozone depleting substances (ODSs) follow the RCP4.5 scenario (van Vuuren et al., 2011), while the quasi-biennial oscillation (QBO) is nudged (see Anet et al., 2013). Each of the ensembles (MEE and NOMEE) consists of 6 members.

3. Results

We focus on the 2002–2005 period, when ionization by MEE is most pronounced.

During the polar night NO_x doesnot get destroyed by photolysis and can be transported by atmospheric winds. In the presence of sunlight, however, its lifetime is only a couple days. Therefore, more pronounced and vertically extensive NO_x enhancement is observed in the winter hemispheres (Fig. 2). In the Southern Hemisphere upper mesosphere the NO_x increase exceeds 40 ppbv (or more than 100% relative to the reference case) and extends down to the stratopause. The magnitude of the simulated NO_x

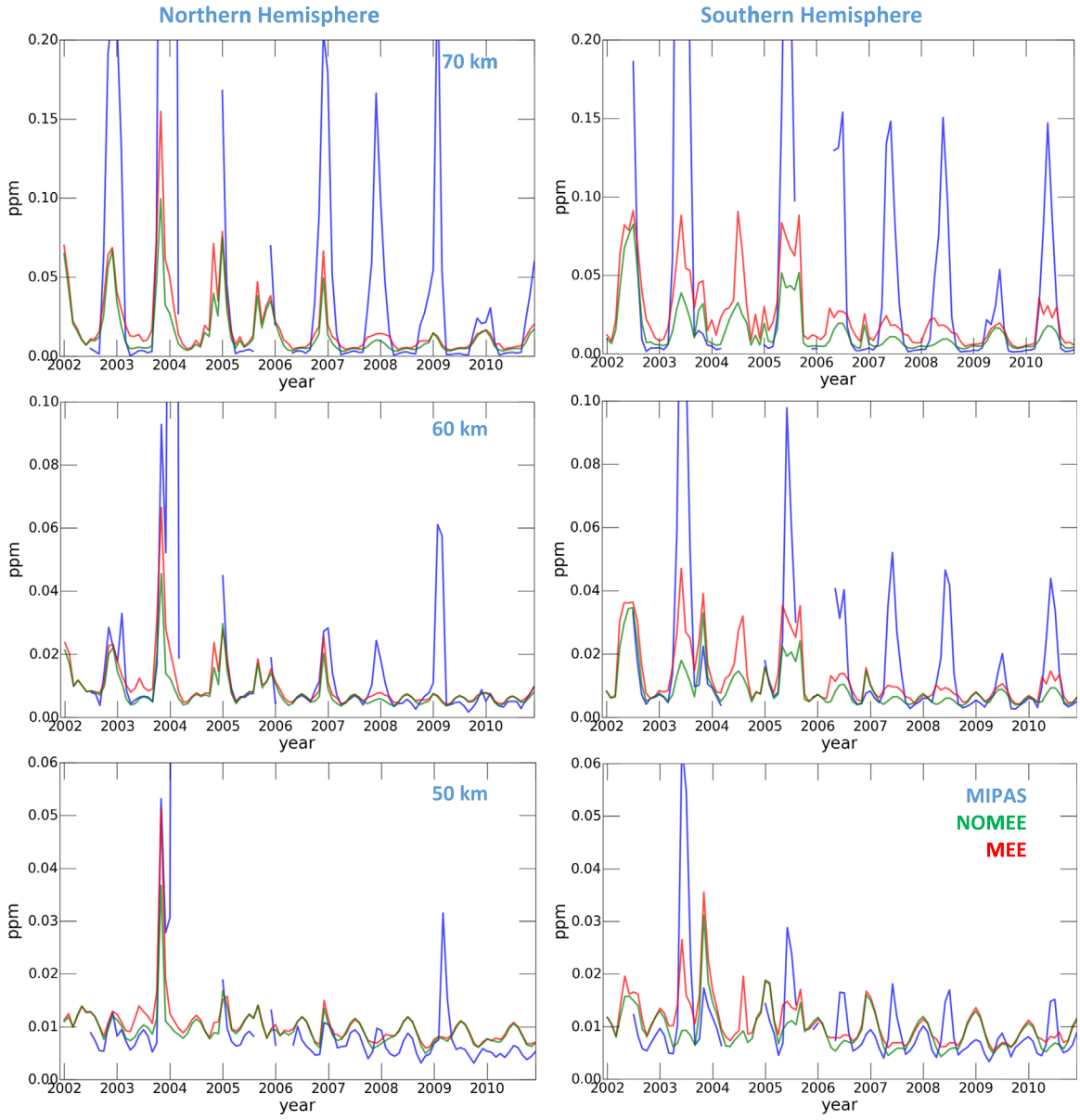

Fig. 6. Comparison between NO_y observations (MIPAS) and MEE/NOMEE simulations at three altitudes – 70, 60 and 50 km for (Left) the Northern Hemisphere (> 70°N average) and (Right) the Southern Hemisphere (> 70°S average).

enhancement is slightly smaller than the 50–150 ppbv simulated by Semeniuk et al. (2011), which is to be expected since we apply much smaller ionization rates. The region of maximum increase is confined to the pole where sunlight is almost completely absent. In the Northern Hemisphere these features are less pronounced due to generally weaker ionization (see Fig. 1) and enhanced horizontal mixing across the vortex edge. Some NO_x enhancement is also visible during the summer season, but mostly in areas outside the polar day zone. The spatial distribution of the NO_x increase at 0.01 hPa (~80 km) is better illustrated in Fig. 3, which suggests that the most pronounced NO_x increase occurs in the regions with highest ionization rates. In winter, the extra NO_x produced by MEE is retained inside the polar vortex and is not depleted because of the lack of photolysis (Funke et al., 2014). In the summer, NO_x is locally produced in regions with high ionization rates, but the presence of sunlight in the Polar Regions leads to intense chemical destruction and less pronounced or even insignificant NO_x increases. Stronger ionization rates in the Southern Hemisphere lead to higher amounts of NO_x than in the Northern Hemisphere in both seasons. The weaker polar vortex in the Northern Hemisphere (Fig. 3a) leads to increased horizontal mixing of NO_x across the vortex and thus a less defined shape compared to the Southern Hemisphere (Fig. 3d).

The seasonal and vertical structure of the MEE NO_x enhancement over the Northern and Southern Polar Regions (60°–90°) is further illustrated in Fig. 4. Additional NO_x production occurs above 64 km in all seasons, but maximizes during winter when sunlight is absent. The stronger wintertime descent inside the southern polar vortex facilitates deeper penetration of NO_x into the stratosphere compared to the Northern Hemisphere (Rozanov et al., 2012). The NO_x reaches down to altitudes of nearly 32 km, albeit the enhancement below 50 km is only marginally significant. The Northern Hemisphere pattern is strongly dominated by the large geomagnetic storms that occurred in November 2003, which resulted in a peak in NO_x enhancement.

Because of its short lifetime, the seasonal and vertical structure of the HO_x response to MEE over the Polar Regions (60°–90°) is only significant in the most upper model level in winter. Increases

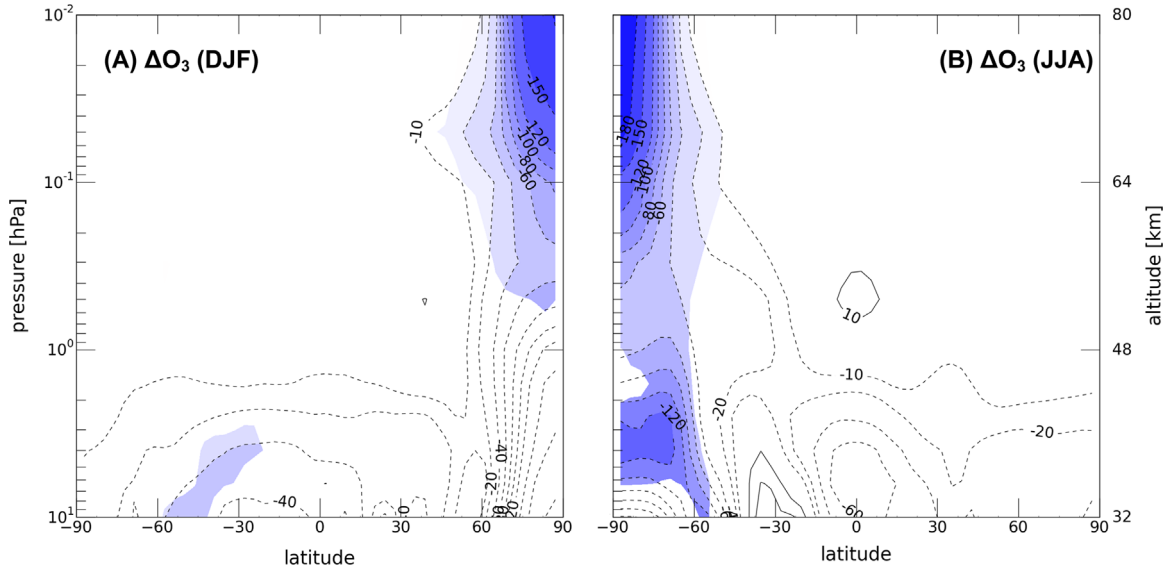

Fig. 7. Zonal mean ozone difference (MEE – NOMEE) in ppbv for DJF (A) and JJA (B) averaged over 2002–2005. Colored regions are significant at the 95% confidence level (calculated using a Student *t*-test). (For interpretation of the references to color in this figure legend, the reader is referred to the web version of this article.)

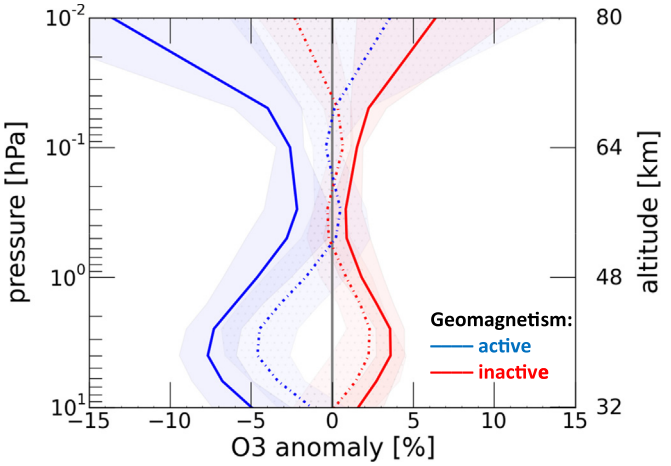

Fig. 8. Vertical profiles of ozone anomalies (%) for geomagnetically active (blue lines; year 2003) and quiet (red lines; 2008-2009 average) periods averaged over 55-65°N geomagnetic latitude. Anomalies are calculated relative to mean winter values (NDJF) for the entire period (2002-2010) for winter). Solid (dashed) lines indicate the ensemble mean from the MEE (NOMEE) simulations. Shading represents the ensemble standard deviation of the anomalies. (For interpretation of the references to color in this figure legend, the reader is referred to the web version of this article.)

of up to 2 ppbv and 6 ppbv are simulated in the Northern and Southern Hemispheres, respectively (not shown).

Some of the first experimental evidence that electron precipitation could produce significant HO_x increase was provided by Verronen et al. (2011) and Andersson et al. (2012). They have shown that the HO_x increase due to particle precipitation is confined to the upper mesosphere (70–78 km altitude). The geographical distribution of the MEE HO_x response at 0.01 hPa is illustrated in Fig. 5; increases of up to 12 ppbv are simulated. This enhancement is only visible in winter and translates to a HO_x increase of up to 45% in the Northern Hemisphere and almost 250% in the Southern Hemisphere. Again, the location of the enhancement corresponds to the location of peak MEE ionization rates. During summer no statistically significant impact on HO_x is seen because of its extremely short lifetime and because the MEE response is masked by photolysis of water vapor. The magnitude of the HO_x increase is lower than the annual mean response of 7 ppbv simulated by Semeniuk et al. (2011), again due to the smaller ionization rates applied in this study.

To evaluate the simulated NO_y ($[N]+[NO]+[NO_2]+2x[N_2O_5]+[HNO_3]+[HNO_4]+[ClNO_3]$) we compare our results with observations from the Michelson Interferometer for Passive Atmospheric Sounding (MIPAS) instrument, which flew onboard the ENVISAT satellite (Funke et al., 2014). Fig. 6 shows NO_y averaged over 70°–90° N/S at 50, 60 and 70 km altitude for both the Northern and Southern Hemisphere. The seasonal cycle of NO_y within the polar caps is driven by a number of processes including in situ chemical production/destruction, exchange with mid-latitudes and in situ production from different precipitating energetic particles, as well as thermospheric NO_x produced by LEE and transported downward during polar winter. The model represents the features of the NO_y seasonal cycle reasonably well. For example, the NO_y enhancements caused by SEP in October 2003 and January 2005 are well simulated. The increase of NO_y after the breakdown of the polar vortex caused by enhanced horizontal transport of NO_y from the mid-latitudes is also captured, as is the wintertime influx of NO_y from the thermosphere. However, the magnitude of these events is not in a good agreement with the satellite observations. The Northern Hemisphere winter 2008/2009 was characterized by weak geomagnetic activity and low ionization rates, while dynamically-initiated major sudden stratospheric warmings in December 2003 and January 2009 led to massive intrusions of thermospheric NO_y into the stratosphere. This event is clearly visible in the MIPAS observations even down to 50 and 60 km (Funke et al., 2014). However, our model in free running mode and at the relatively low horizontal resolution does not properly simulate such events. The NO_y peaks in October 2003 and January 2005 are caused by SPE, which are underestimated in the model simulation except at 50 km. However, at this altitude, the modeled NO_y shows less sensitivity to the ionization rates, and simulated NO_y is overestimated compared to MIPAS observations during this geomagnetically inactive period. The inclusion of MEE improves the representation of NO_y at 60 and 70 km, particularly during geomagnetically active periods; however, substantial underestimation of NO_y during winter remains an issue. This requires the development of new parameterizations for the treatment of NO_y influx from the thermosphere.

A simulation without energetic particles (not shown) suggests that almost all NO_y at 70 and 60 km results from energetic

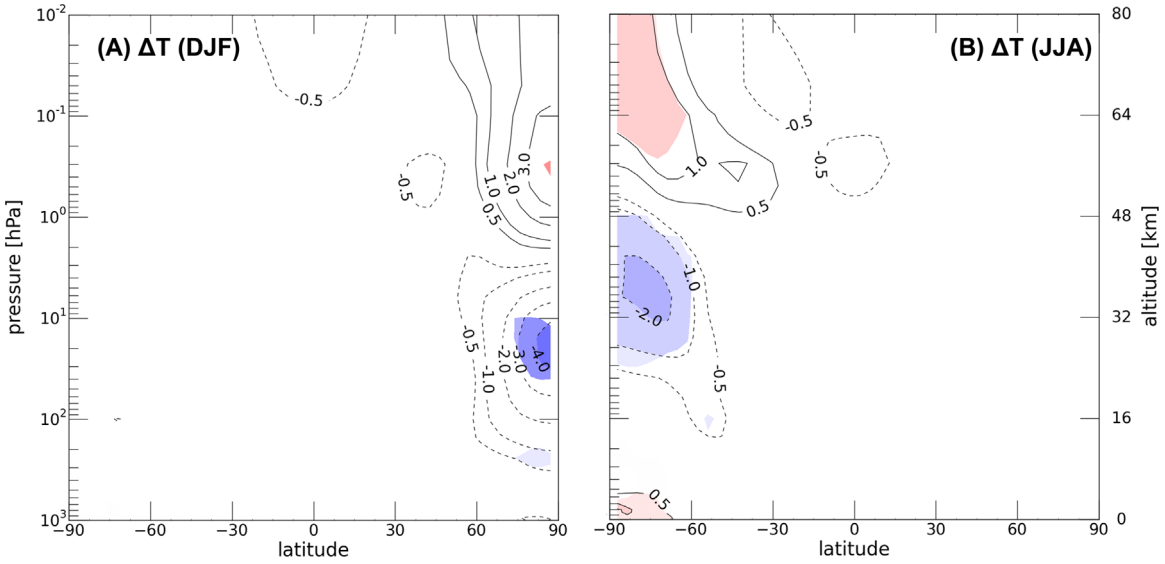

Fig. 9. Zonal mean temperature difference (MEE – NOMEE) in K for DJF (A) and JJA (B) averaged over 2002–2005. Colored regions are significant at the 95% confidence level (calculated using a Student *t*-test). (For interpretation of the references to color in this figure legend, the reader is referred to the web version of this article.)

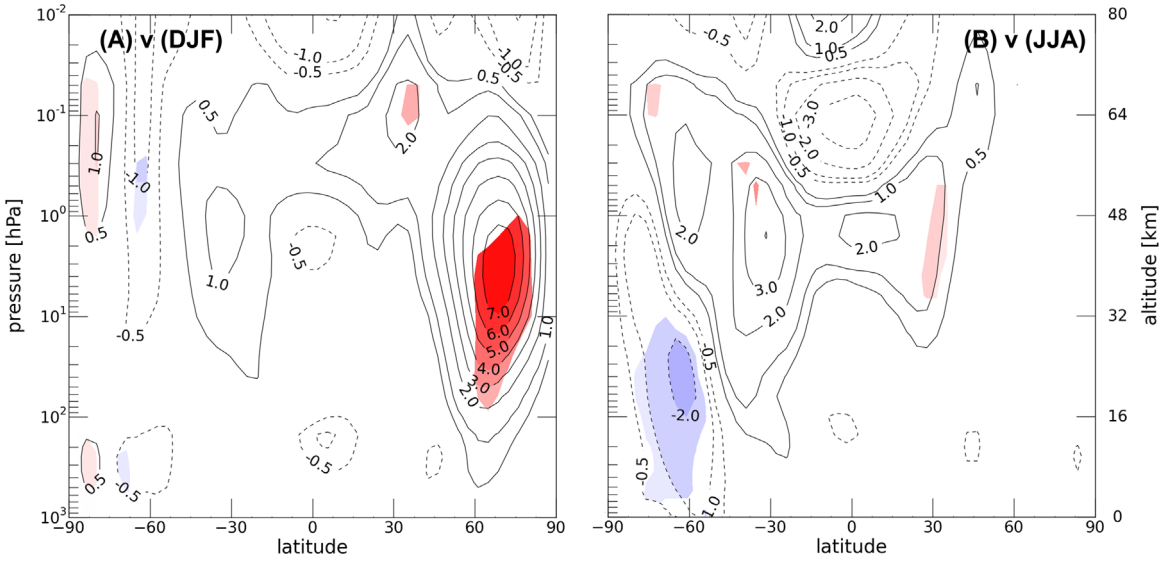

Fig. 10. Zonal mean wind difference (MEE – NOMEE) in m/s for DJF (A) and JJA (B) averaged over 2002–2005. Colored regions are significant at the 95% confidence level (calculated using a Student *t*-test). (For interpretation of the references to color in this figure legend, the reader is referred to the web version of this article.)

particles; their exclusion from the model would lead to a significant underestimation of NO_y and thus an overestimation of ozone at these altitudes.

Fig. 7 illustrates seasonal changes in ozone mixing ratios resulting from MEE. The main ozone loss occurs in the upper mesosphere (70-80 km altitude) and is driven by reactions involving the NO_x and HO_x families (Sinnhuber et al., 2012). MEE strongly impact ozone in the Southern Hemisphere during winter (JJA) where ozone depletion reaches up to 200 ppbv (about 40%) in the upper mesosphere and up to 120 ppbv (~2.5%) in the upper stratosphere. In the Northern Hemisphere winter ozone depletion is slightly smaller, reaching 150 ppbv (about 25%) in the upper mesosphere. Ozone depletion is also visible down to the upper stratosphere, but is not statistically significant below 1 hPa. Semeniuk et al. (2011) found even larger ozone decreases in the mesosphere in response to MEE (more than 1 ppbv or up to 80% during austral winter), which, again, can be explained by larger ionization rates used.

Following Andersson et al. (2014) we compare vertical profiles of ozone anomalies in the Northern Hemisphere during geomagnetically active (2003/2004) and inactive (2008/2009 and 2009/2010) periods (Fig. 8). Anomalies are calculated compared to a climatology from all winter seasons (NDJF) over the 2002–2010 period and averaged over the auroral oval (55°–70°N). During active periods there is up to 15% less ozone in the upper mesosphere and up to 8% less in the upper stratosphere. Without MEE, anomalies shows large variability between ensemble members and on average do not exceed 5% in the upper stratosphere. In contrast, during inactive periods, there is a positive ozone anomaly in the upper mesosphere of up to 5% and up to 3% in the upper stratosphere. Andersson et al. (2014) used satellite observations and also found similar MEE impacts on ozone, with negative ozone anomalies (up to 15%) in the mesosphere during active periods and positive anomalies in the mesosphere during inactive years (again up to 15%), which emphasizes the importance of MEE for the atmospheric chemistry.

Winter zonal mean temperature and zonal wind changes resulting from MEE are shown in Figs. 9 and 10, respectively. Ozone

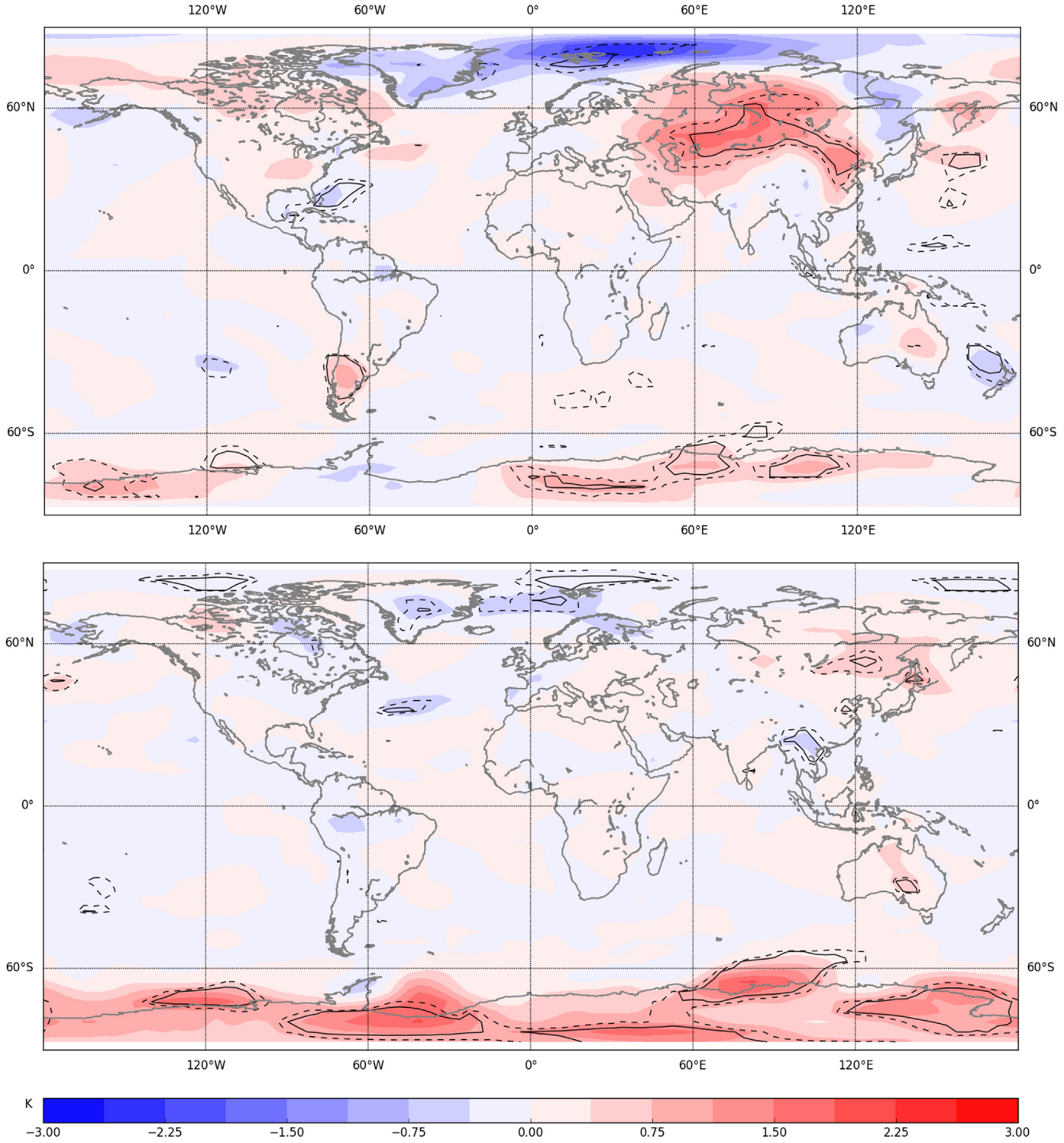

Fig. 11. Spatial distribution of 2 m temperature difference (MEE – NOMEE) in K for DJF (upper plot) and JJA (lower plot) averaged over 2002–2005. Dashed line circles the regions with 90% and solid line with the 95% confidence level (calculated using a Student *t*-test).

loss confined to the layers above 1 hPa during all winter months (see Fig. 7) leads to lower heating rates and colder temperatures in the sunlit part of the high latitudes, which is not compensated by the small warming induced by the decrease of infrared cooling rates (see Karami et al., 2015). This cooling provides the necessary conditions for the statistically significant acceleration of the winter mean northern polar vortex by up to 7 m/s. A stronger polar vortex leads to the intensification of the descent and adiabatic warming in the mesosphere (e.g., Limpasuvan et al., 2005), which compensates for the initial cooling due to ozone depletion. As a result, the temperature changes above 1 hPa are only marginally significant. In the middle stratosphere acceleration of the zonal winds prevents horizontal heat and species transport leading to cooling and ozone reduction (albeit not significant). The same processes operate over the Southern Hemisphere, however due to the stronger and more stable vortex the changes are slightly less significant and shifted downwards. Semeniuk et al. (2011) found a significant equatorward shift of the Northern Hemisphere polar

vortex, with simultaneous significant decreases in temperature of up to 1 K near 50–60°N in the lower stratosphere and increases of up to 1 K above the stratopause. These features are consistent with our results, but the locations of the significant changes are slightly different. In austral winter we find conflicting results. Whereas Semeniuk et al. (2011) show warming in the stratosphere and cooling (both up to 3 K) in the mesosphere, our model simulates the opposite response. Our results are, however, consistent with the acceleration of the polar vortex. Using the ERA reanalysis, Seppälä et al. (2013) also found that high geomagnetic activity can drive a strengthening of the Northern Hemisphere polar vortex, with warming in the polar upper stratosphere and cooling below. A further study (Karami et al., 2015) showed a similar temperature response to our results in the Southern Hemisphere, but a reversed in sign for the Northern Hemisphere. However, direct comparison is not possible because the ozone perturbations scenario used for their study is different from the ozone response simulated with our model. Additionally, our results indicate significant warming over Antarctica in the lower troposphere of up to 1 K.

MEE precipitation influences not only chemistry and climate in the upper atmosphere, but also the surface climate. Intensification of the polar vortex is known to force a positive phase of the Northern/Southern Annular modes (Limpasuvan et al., 2005). In the Northern Hemisphere the positive phase of the Northern Annular Mode (NAM) results in cooling of the Polar Regions and warming of up to 2 K over continental Asia (Fig. 11). A positive temperature anomaly is also seen over Northern America, however this is not statistically significant. A recent study by Chiodo et al. (2016) confirmed this mechanism by showing that the cooling of the tropical stratosphere due to the decrease in UV radiation leads to a weakening of the Northern Hemisphere polar vortex, a negative phase of NAM, and thus warming in the Polar Region and simultaneous cooling in mid-latitudes.

During austral winter an increase of sea level pressure over Antarctica leads to a deceleration of westerly winds around 60 ° S and thus a negative phase of Southern Annular Mode (SAM). This effect induces warming of up to 3 K over Antarctica (Kwok and Comiso, 2002), which can influence ice melt over longer timescales. Further investigation of this effect is beyond the scope of this paper. If the model accurately reproduces observed NO_y, ozone depletion will likely be larger leading to larger thermal and dynamical responses in the middle atmosphere and amplification of the simulated surface signal.

4. Conclusions

During geomagnetically active periods (e.g. 2002-2005), MEE (with energies ranging 30-300 keV) lead to significant increases of NO_x (up to 150%) and HO_x (up to 250%) in the polar mesosphere, which in turn result in ozone depletion. Ozone decreases are particularly evident during geomagnetically active years over the auroral oval (55°–70°N/S) when negative anomalies of up to 15% and 8% are seen in the mesosphere and stratosphere, respectively, compared to the climatological mean state. Dynamical changes are also seen during winter, with an intensification of the polar vortex and negative temperature anomalies in the middle stratosphere. Furthermore, a significant surface temperature response is detected over Antarctica during austral winter and over central and eastern Asia during boreal winter. The comparison of simulated NO_x with MIPAS data showed that the implementation of a parameterization to represent MEE improves the agreement, especially during geomagnetically active periods. However, a substantial underestimation of winter NO_x above 50 km even during the quiet periods remains. This model deficiency can be explained by the underestimation of the downward flux of NO_x from the thermosphere and calls for an improvement of the parameterization applied here. A new parameterization is required to better simulate the magnitude of potential NO_x decreases, particularly during periods of low solar activity relative to present day conditions. MEE produce thermal and dynamical changes in the atmosphere, even down to the surface, and are thus potentially of importance to climate change. Our results indicate that the inclusion of MEE in chemistry-climate models is crucial.

Acknowledgments

This work has been supported by the Swiss National Science Foundation under Grant CRSII2-147659 (FUPSOL II). F. Tummon has been supported by the Swiss National Science Foundation under Project 20FI21_138017. This work is a part of ROSMIC WG1 activity within the SCOSTEP VarSITI program. We would also like to acknowledge the financial support by the Academy of Finland to the ReSoLVE Centre of Excellence (project no. 272157). We thank Aleš Kuchař from Charles University, Prague, Czech Republic for assistance with improving the graphics.

References

Aikin, A., 1994. Energetic particle-induced enhancement of stratospheric nitric acid. Geophys. Res. Lett. 21 (10), 859–862.

Andersson, M.E., Verronen, P.T., Rodger, C.J., Cliverd, M.A., Seppälä, A., 2014. Missing driver in the Sun–Earth connection from energetic electron precipitation impact mesospheric ozone. Nat. Commun. http://dx.doi.org/10.1038/ncomms6197

Andersson, M.E., Verronen, P.T., Wang, S., Rodger, S.J., Clilverd, M.A., Carson, B., 2012. Precipitating radiation belt electrons and enhancements of mesospheric hydroxyl during 2004–2009. J. Geophys. Res. 117, D09304. http://dx.doi.org/10.1029/2011JD017246.

Anet, J.G., Muthers, S., Rozanov, E., Raible, C.C., Peter, T., Stenke, A., Shapiro, A.I., Beer, J., Steinhilber, F., Brönnimann, S., Arfeuille, F., Brugnara, Y., Schmutz, W., 2013. Forcing of stratospheric chemistry and dynamics during the Dalton minimum. Atmos. Chem. Phys. 13, 15061–15104. http://dx.doi.org/10.5194/acpd-13-15061-2013 2013. 6183, 6184, 6187, 6189, 6190, 6191, 6201, 6202.

Baker, D.N., Goldberg, R.A., Herrero, F.A., Blake, J.B., Callis, L.B., 1993. Satellite and rocket studies of relativistic electrons and their influence on the middle atmosphere. J. Atmos. Terr. Phys. 55, 1619–1628.

Baker, D.N., Barth, C.A., Mankoff, K.E., Kanekal, S.G., Bailey, S.M., Mason, G.M., Mazur, J.E., 2001. Relationships between precipitating auroral zone electrons and lower thermospheric nitric oxide densities: 1998–2000. J. Geophys. Res. 106 (A11), 24465–24480. http://dx.doi.org/10.1029/2001JA000078.

Barth, C.A., Mankoff, K.D., Balley, S.M., Solomon, S.C., 2003. Global observations of nitric oxide in the thermosphere. J. Geophys. Res. 108, 1027. http://dx.doi.org/10.1029/2002JA009458.

Baumgaertner, A.J.G., Jöckel, P., Brühl, C., 2009. Energetic particle precipitation in ECHAM5/MESSy1 – Part 1: Downward transport of upper atmospheric NO_x produced by low energy electrons. Atmos. Chem. Phys. 9, 2729–2740. http://dx.doi.org/10.5194/acp-9-2729-2009 2009. 6188.

Baumgaertner, A.J.G., Seppälä, A., Jöckel, P., Clilverd, M.A., 2011. Geomagnetic activity related NO_x enhancements and polar surface air temperature variability in a chemistry climate model: modulation of the NAM index. Atmos. Chem. Phys. 11, 4521–4531. http://dx.doi.org/10.5194/acp-11-4521-2011.

Bazilevskaya, G.A., Usoskin, I.G., Flückiger, E.O., Harrison, R.G., Desorgher, L., Bütikofer, R., Krainev, M.B., Makhmutov, V.S., Stozhkov, Y.I., Svirzhevskaya, A.K., Svirzhevsky, N.S., Kovaltsov, G.A., 2008. Cosmic ray induced ion production in the atmosphere. Space Sci. Rev. 137 149–17.

Brasseur, G., Solomon, S., 2005. Aeronomy of the Middle Atmosphere: Chemistry and Physics of the Stratosphere and Mesosphere, third ed. Springer, Dordrecht, the Netherlands.

Calisto, M., Usoskin, I., Rozanov, E., Peter, T., 2011. Influence of galactic cosmic rays on atmospheric composition and dynamics. Atmos. Chem. Phys. 11, 4547–4556. http://dx.doi.org/10.5194/acp-11-4547-2011.

Cane, H.V., Mewaldt, R.A., Cohen, C.M.S., von Rosenvinge, T.T., 2006. Role of flares and shocks in determining solar energetic particle abundances. J. Geophys. Res. 111, A06S90. http://dx.doi.org/10.1029/2005JA011071.

Chiodo, G., Garcia-Herrera, R., Calvo, N., Vaquero, J.M., Anel, J.A., Barriopedro, D., Matthes, K., 2016. The impact of a future solar minimum on climate change projections in the Northern Hemisphere. Environ. Res. Lett. 11, 034015. http://dx.doi.org/10.1088/1748-9326/11/3/034015 2016(2016).

Codrescu, M.V., Fuller-Rowell, T.J., 1997. Medium energy particle precipitation influence on the mesosphere and lower thermosphere. J. Geophys. Res. 102 (A9)

19977–1987.
Crutzen, P.J., 1975. Solar proton events: stratospheric sources of nitric oxide. Science 189, 457–459.
Degestin, D.A., Lloyd, N.D., Bourassa, A.E., Gattinger, R.L., Llewellyn, E.J., 2005. Observations of mesospheric ozone depletion during the october 28, 2003 solar proton event by OSIRIS. Geophys. Res. Lett. 32, L03S11. http://dx.doi.org/10.1029/2004GL021521.
Dorman, L.I., 2004. Cosmic Rays in the Earth's Atmosphere and Underground. Kluwer, Dordrecht.
Egorova, T., Rozanov, E., Zubov, V., Karol, I., 2003. Model for Investigating Ozone Trends (MEZON), Izvestiia Akademii Nauk SSSR. Ser. Fiz. Atmos. Okean. 39, 310–326 6186.
Egorova, T., Rozanov, E., Ozolin, Y., Shapiro, A., Calisto, M., Peter, T., Schmutz, W., 2011. The atmospheric effects of october 2003 solar proton event simulated with the chemistry–climate model SOCOL using complete and parameterized ion chemistry. J. Atmos. Solar. Terr. Phys 73, 356–365. http://dx.doi.org/10.1016/j.jastp.2010.01.009.
Finlay, C.C., et al., 2010. International Geomagnetic Reference Field: the eleventh generation. Geophys. J. Int. 183 (3), 1216–1230. http://dx.doi.org/10.1111/j.1365-246X.2010.04804.x.
Funke, B., López-Puertas, M., Stiller, G.P., von Clarmann, T., 2014. Mesospheric and stratospheric NO_y produced by energetic particle precipi- tation during 2002–2012. J. Geophys. Res. Atmos. 119, 4429–4446. http://dx.doi.org/10.1002/2013JD021404.
Funke, B., Baumgaertner, A., Calisto, M., Egorova, T., Jackman, C.H., Kieser, J., Krivolutsky, A., López- Puertas, M., Marsh, D.R., Reddmann, T., Rozanov, E., Salmi, S.-M., Sinnhuber, M., Stiller, G.P., Verronen, P.T., Versick, S., von Clarmann, T., Vyushkova, T.Y., Wieters, N., Wissing, J.M., 2011. Composition changes after the Halloween solar proton event: The High Energy Particle Precipitation in the Atmosphere (HEPPA) model versus MIPAS data intercomparison study. Atmos. Chem. Phys. 11, 9089–9139. http://dx.doi.org/10.5194/acp-11-9089-2011.
Grieder, P.K.F., 2001. Cosmic Rays at Earth: Researcher's Reference Manual and Data Book. Elsevier, Amsterdam.
IPCC, 2013: Climate Change 2013: The Physical Science Basis. Contribution of Working Group I to the Fifth Assessment Report of the Intergovernmental Panel on Climate Change [Stocker, T.F., D. Qin, G.-K. Plattner, M. Tignor, S.K. Allen, J. Boschung, A. Nauels, Y. Xia, V. Bex and P.M. Midgley (eds.)]. Cambridge University Press, Cambridge, United Kingdom and New York, NY, USA, 1535 pp.
Jackman, C., Marsh, D.R., Kinnison, D.E., Mertens, C.J., Fleming, E.L., 2015. Atmospheric changes caused by galactic cosmic rays over the period 1960–2010. Atmos. Chem. Phys. Discuss 15, 33931–33966. http://dx.doi.org/10.5194/acpd-15-33931-2015.
Jackman, C.H., Marsh, D.R., Vitt, F.M., Garcia, R.R., Randall, C.E., Fleming, E.L., Frith, S. M., 2009. Long-term middle atmospheric influence of very large solar proton events. J. Geophys. Res. 114, D11304.
Jackman, C.H., Marsh, D.R., Vitt, F.M., Garcia, R.R., Fleming, E.L., Labow, G.J., Randall, C.E., López-Puertas, M., Funke, B., von Clarmann, T., Stiller, G.P., 2008. Short- and medium-term atmospheric constituent effects of very large solar proton events. Atmos. Chem. Phys. 8, 765–785. http://dx.doi.org/10.5194/acp-8-765-2008.
Jungclaus, J.H., Keenlyside, N., Botzet, M., Haak, H., Luo, J.J., Latif, M., Marotzke, J., Mikolajewicz, U., Roeckner, E., 2006. Ocean circulation and tropical variability in the coupled model ECHAM5/MPI-OM. J. Clim. 19, 3952–3972. http://dx.doi.org/10.1175/JCLI3827.1 3021.
Karami, K., Braesicke, P., Kunze, M., Langematz, U., Sinnhuber, M., Versick, S., 2015. Modelled thermal and dynamical responses of the middle atmosphere to EPP-induced ozone changes. Atmos. Chem. Phys. Discuss. 15, 33283–33329. http://dx.doi.org/10.5194/acpd-15-33283-2015.
Kwok, R., Comiso, J.C., 2002. Spatial patterns of variability in Antarctic surface temperature: Connections to the Southern Hemisphere Annular Mode and the Southern Oscillation. J. Geophys. Res 29, 14. http://dx.doi.org/10.1029/2002GL015415.
Limpasuvan, V., Hartmann, D.L., Thompson, D.L.H., Jeev, K., Yung, Y.L., 2005. Stratosphere-troposphere evolution during polar vortex intensification. J. Geophys. Res. 110, D24101. http://dx.doi.org/10.1029/2005JD006302.
Marsland, S., 2003. The Max-Planck-Institute global ocean/sea ice model with orthogonal curvilinear coordinates. Ocean Model. 5, 91–127. http://dx.doi.org/10.1016/S1463-5003(02)00015-X 3021.
Muthers, S., Anet, J.G., Stenke, A., Raible, C.C., Rozanov, E., Brönnimann, S., Peter, T., Arfeuille, F.X., Shapiro, A.I., Beer, J., Steinhilber, F., Brugnara, Y., Schmutz, W., 2014. The coupled atmosphere-chemistry-ocean model SOCOL-MPIOM. Geosci. Model Dev. 7, 3013–3084. http://dx.doi.org/10.5194/gmdd-7-3013-2014.
Nicolet, M., 1965. Ionospheric processes and nitric oxide. J. Geophys. Res. 70, 691–701.
Nicolet, M., 1975. On the production of nitric oxide by cosmic rays in the mesosphere and stratosphere. Planet. Space Sci. 23, 637–649.
Nieder, H., Winkler, H., Marsh, D.R., Sinnhuber, M., 2014. NO_x production due to energetic particle precipitation in the MLT region: Results from ion chemistry model studies. J. Geophys. Res. Space Phys. 119, 2137–2148. http://dx.doi.org/10.1002/2013JA019044.
Reames, D., 1999. Particle acceleration at the sun and in the heliosphere. Space Sci. Rev. 90, 413–491.
Roeckner, E., Bäuml, G., Bonaventura, L., Brokopf, R., Esch, M., Giorgetta, M., Hagemann, S., Kirchner, L., Kornblueh, L., Manzini, E., Rhodin, A., Schlese, U., Schulzweida, U., Tompkins, A., 2003. The Atmospheric General Circulation Model ECHAM5-Model Description. Max-Planck Institute for Meteorology, Hamburg, Germany (MPI report 349).
Rozanov, E., Schlesinger, M.E., Zubov, V., Yang, F., Andronova, N.G., 1999. The UIUC three-dimensional stratospheric chemical transport model: description and evaluation of the simulated source gases and ozone. J. Geophys. Res. 104, 755–781. http://dx.doi.org/10.1029/1999JD900138 6186.
Rozanov, E., Calisto, M., Egorova, T., Peter, T., Schmutz, W., 2012. Influence of the precipitating energetic particles on atmospheric chemistry and climate. Surv. Geophys. 33, 483–501. http://dx.doi.org/10.1007/s10712-012-9192-0 3021.
Rusch, D., Gerard, G.-C., Solomon, S., Crutzen, P., Reid, G., 1981. The effect of particle precipitation events on the neutral and ion chemistry of the middle atmosphere. 1. Odd nitrogen. Planet. Space Sci. 29, 767–774.
Semeniuk, K., Fomichev, V.I., McConnell, J.C., Fu, C., Melo, S.M.L., Usoskin, I.G., 2011. Middle atmosphere response to the solar cycle in irradiance and ionizing particle precipitation. Atmos. Chem. Phys., 11. http://dx.doi.org/10.5194/acp-11-5045-2011.
Seppälä, A., Lu, H., Clilverd, M.A., Rodger, C.J., 2013. Geomagnetic activity signatures in wintertime stratosphere wind, temperature, and wave response. J. Geophys. Res. Atmos. 118, 2169–2183. http://dx.doi.org/10.1002/jgrd.50236.
Seppälä, A., Randall, C.E., Clilverd, M.A., Rozanov, E., Rodger, C.J., 2009. Geomagnetic activity and polar surface air temperature variability. JGR 114, A10312. http://dx.doi.org/10.1029/2008JA014029.
Sinnhuber, M., Nieder, H., Wieters, N., 2012. Energetic particle precipitation and the chemistry of the meso- sphere/lower thermosphere. Surv. Geophys. 33, 1281–1334. http://dx.doi.org/10.1007/s10712-012-9201-3.
Solomon, S., Rusch, D.W., Gerard, J.-C., Reid, G.C., Crutzen, P.J., 1981. The effect of particle precipitation events on the neutral and ion chemistry of the middle atmosphere, II, Odd hydrogen. Planet. Space Sci. 29 (8), 885–892.
Solomon, Susan, Crutzen, P.J., Roble, R.G., 1982. Photochemical coupling between the thermosphere and the lower atmosphere 1. Odd nitrogen from 50 to 120 km. J. Geophys. Res. 87, 7206–7220. http://dx.doi.org/10.1029/JC087iC09p07206.
Steinhilber, F., Beer, J., 2013. Prediction of solar activity for the next 500 years. J. Geophys. Res.: Space Phys. 118, 1861–1867. http://dx.doi.org/10.1002/jgra.50210.
Stenke, A., Schraner, M., Rozanov, E., Egorova, T., Luo, B., Peter, T., 2013. The SOCOL version 3.0 chemistry–climate model: description, evaluation, and implications from an advanced transport algorithm. Geosci. Model Dev. 6, 1407–1427. http://dx.doi.org/10.5194/gmd-6-1407-2013, 2013b. 3019, 3031, 3036.
Swider, W., Keneshea, T.J., 1973. Decrease of ozone and atomic oxygen in the lower mesosphere during a PCA event. Planet. Space Sci. 21, 1969–1973.
Turunen, E., Verronen, P.T., Seppälä, A., Rodger, C.J., Clilverd, M.A., Tamminen, J., Enell, C.F., Ulich, T., 2009. Impact of different energies of precipitating particles on NO_x generation in the middle and upper atmosphere during geomagnetic storms. J Atmos Sol Terr Phy 71, 1176–1189, doi:10,1016/j.jastp. 2008.07.05.
Usoskin, I.G., Kovaltsov, G.A., Mironova, I.A., 2010. Cosmic ray induced ionization model CRAC:CRII: an extension to the upper atmosphere. J. Geophys. Res. 115, D10302. http://dx.doi.org/10.1029/2009JD013142.
Van Vuuren, D.P., Edmonds, J., Kainuma, M., Riahi, K., Thomson, A., Hibbard, K., Hurtt, C., Kram, T., Krey, V., Lamarque, J.-F., Masui, T., Meinhausen, M., Nakicenovic, N., Smith, S.J., Rose, S.K., 2011. The representative concentration pathways: an overview. Clim. Chang. 109, 5–31. http://dx.doi.org/10.1007/s10584-011-0148-z (2011).
Verronen, P.T., Rodger, C.J., Clilverd, M.A., Wnag, S., 2011. First evidence of mesospheric hydroxil response to electron precipitation from the radiation belts. J. Geophys. Res. 116, D07307. http://dx.doi.org/10.1029/2010JD014965.
Weeks, L.H., CuiKay, R.S., Corbin, R.J., 1972. Ozone measurements in the mesosphere during the solar proton event of 2 November 1969. J. Atmos. Sci. 29, 1138–1142.
Wissing, J.M., Kallenrode, M.-B., 2009. Atmospheric Ionization Module Osnabrück (AIMOS): a 3-D model to determine atmospheric ionization by energetic charged particles from different populations. J. Geophys. Res., 114. http://dx.doi.org/10.1029/2008JA013884.
Yando, K., Millan, R.M., Green, J.C., Evans, D.S., 2011. A Monte Carlo simulation of the NOAA POES medium energy proton and electron detector instrument. J. Geophys. Res. 116, A10231. http://dx.doi.org/10.1029/2011JA016671.